electrochem

MDPI

Article

Effect of Recombinant Antibodies and MIP Nanoparticles on the Electrical Behavior of Impedimetric Biorecognition Surfaces for SARS-CoV-2 Spike Glycoprotein: A Short Report

Douglas Vieira Thomaz [1,*], Riccardo Goldoni [2,3], Gianluca Martino Tartaglia [4,5], Cosimino Malitesta [1] and Elisabetta Mazzotta [1,*]

1 Dipartimento di Scienze e Tecnologie Biologiche e Ambientali, Università del Salento, 73100 Lecce, Italy
2 Department of Electronics, Information and Bioengineering, Politecnico di Milano, 20133 Milan, Italy
3 National Research Council, Institute of Electronics, Computer and Telecommunication Engineering (CNR-IEIIT), 20133 Milan, Italy
4 Department of Biomedical, Surgical and Dental Sciences, School of Dentistry, University of Milan, 20100 Milan, Italy
5 UOC Maxillo-Facial Surgery and Dentistry Fondazione IRCCS Cà Granda, Ospedale Maggiore Policlinico, 20122 Milan, Italy
* Correspondence: douglasvthomaz@gmail.com (D.V.T.); elisabetta.mazzotta@unisalento.it (E.M.)

Abstract: Electrochemical immunosensors are often described as innovative strategies to tackle urgent epidemiological needs, such as the detection of SARS-CoV-2 main biomarker, the spike glycoprotein. Nevertheless, there is a great variety of receptors, especially recombinant antibodies, that can be used to develop these biosensing platforms, and very few reports compare their suitability in analytical device design and their sensing performances. Therefore, this short report targeted a brief and straightforward investigation of the performance of different impedimetric biorecognition surfaces (BioS) for SARS-CoV-2, which were crafted from three commonly reported recombinant antibodies and molecularly-imprinted polymer (MIP) nanoparticles (nanoMIP). The selected NanoMIP were chosen due to their reported selectivity to the receptor binding domain (RBD) of SARS-CoV-2 spike glycoprotein. Results showed that the surface modification protocol based on MUDA and crosslinking with EDC/NHS was successful for the anchoring of each tested receptor, as the semicircle diameter of the Nyquist plots of EIS increased upon each modification, which suggests the increase of R_{ct} due to the binding of dielectric materials on the conductive surface. Furthermore, the type of monoclonal antibody used to craft the BioS and the artificial receptors led to very distinct responses, being the RBD5305 and the NanoMIP-based BioS the ones that showcased the highest increment of signal in the conditions herein reported, which suggests their adequacy in the development of impedimetric immunosensors for SARS-CoV-2 spike glycoprotein.

Keywords: covid; coronavirus; biosensor; electrochemistry; immunosensors; molecularly-imprinted polymer

check for updates

Citation: Thomaz, D.V.; Goldoni, R.; Tartaglia, G.M.; Malitesta, C.; Mazzotta, E. Effect of Recombinant Antibodies and MIP Nanoparticles on the Electrical Behavior of Impedimetric Biorecognition Surfaces for SARS-CoV-2 Spike Glycoprotein: A Short Report. *Electrochem* **2022**, *3*, 538–548. https://doi.org/10.3390/electrochem3030037

Academic Editor: Masato Sone

Received: 29 July 2022
Accepted: 25 August 2022
Published: 2 September 2022

1. Introduction

The advent of the SARS-CoV-2 pandemic led many researchers to develop new biosensing technologies, amongst which electrochemistry thrived as a reliable and affordable way to promote point-of-need testing [1]. This technology is based on the intrinsic electric properties of matter and allows for the determination of the concentration of compounds either through the electric current that is generated from redox processes, or changes in the electric behavior of the sensing surface [2–4]. The performance of electroanalytical detection has been compared to standard analytical techniques based on spectrophotometry, as well as other optical physics approaches such as surface plasmon polaritons, Kretschmann configurations, and extraordinary optical transmission, allowing it to be used either as a

complimentary method or standalone biosensing technology [5,6]. In this regard, numerous authors detailed the use of voltammetry and electrochemical impedance spectroscopy (EIS) as analytical techniques in the detection and quantification of SARS-CoV-2 antigens, such as its spike and nucleoproteins [7]. To all accounts, these technologies allowed the crafting of portable sensing platforms whose performance often rivalled highly refined diagnostic tools.

Moreover, novel point-of-care (POC) devices are designed to be flexible in terms of the biofluids being analyzed. While blood still retains its role as the gold standard for diagnostic purposes, several alternative body fluids have already been explored, giving encouraging results for noninvasive rapid testing [8]. Among these, saliva has been identified as a promising candidate for disease diagnostics due to its rich availability in biomarkers, continuous renovation, and ease of collection [9]. Salivary biomarkers have been already identified for several pathologies, such as cancer [10], neurodegenerative diseases [11], and systemic diseases [12]. Viral infections constitute another challenging target that salivary analysis could tackle, and some examples already surfaced relative to SARS-CoV-2 [13] detection.

Although the development of electrochemical biosensing devices for SARS-CoV-2 has been extensively demonstrated and validated by researchers worldwide [14], the approaches taken in these studies were vastly distinct. While the majority of authors resorted to the detection of the spike glycoprotein, some works concerned the detection of the nucleoprotein through a range of recombinant antibodies [15,16]. Even though these differences may not pose an issue at first glance, it must be noted that there is a long list of recombinant antibodies for SARS-CoV-2 antigens, and each combination yields different binding responses, which can have deep implications on the reliability of the sensor [17,18].

Intrinsic to the use of antibodies in biosensing applications are their limitations in terms of stability. It is well reported that the sensing platform must be carefully crafted and optimized in order to reach adequate stability [19]. On the same hand, researchers have to carefully consider which reagents, solvents, and conditions shall be taken during the surface modification of the sensing substrate; hence most biological macromolecules have a narrow stability range in regards to the physicochemical features of the environment where they are placed [20]. In fact, these limitations led to the selection of a small number of anchoring and crosslinking protocols that can be performed within a physiological medium, without extreme heating or shifts in the acidity/alkalinity of the environment.

Owing to the vast number of recombinant antibodies for SARS-CoV-2, and their varied binding behavior to the antigens, as well as the limited stability of these molecules, some groups have proposed the use of artificial receptors, namely molecularly imprinted polymers nanoparticles (NanoMIP) in the development of reliable and robust biosensing platforms [21–23]. Molecular imprinting technologies are based on the topological imprinting of targets on the surface of a polymer, thereby leading to a cavity of shape and size equal to that of the target [24,25]. This very feature grants MIP-based sensors their acknowledged selectivity, while the polymer nature confers stability due to the inherent robustness of polymeric networks [26]. Indeed, several authors detailed the benefits of applying MIP and NanoMIP in sensing technologies, and some reported their application in the development of MIP-based SARS-CoV-2 immunosensors [27,28], thus paving the way for the development of innovative analytical platforms to address urgent needs in medicine.

Considering the need to better understand how the responses of recombinant antibodies vary in bioanalytical applications, and also how MIP technologies stand in comparison to these approaches, this short report targeted a straightforward investigation and comparison of the performance of different BioS based on impedimetric detection for SARS-CoV-2, which were crafted from three commonly reported recombinant antibodies, and commercial NanoMIP. The selected NanoMIP were chosen due to their reported selectivity to the receptor binding domain (RBD) of SARS-CoV-2 spike glycoprotein. We hope our investigation sheds light on the importance of the adequate selection of recombinant antibodies in

the development of biosensing technologies, as well as showcasing the benefits of using NanoMIP in sensing applications.

2. Materials and Methods

2.1. Reagents and Solutions

The salts NaCl, KCl, Na_2HPO_4, and KH_2PO_4 were used to prepare a phosphate-buffered saline (PBS), pH 7.4. 11-mercaptoundecanoic acid (MUDA) was prepared into an ethanolic solution at 10 mmol·L^{-1}, while the solutions of N-ethyl-N′-(3-(dimethylamino) propyl) carbodiimide and N-hydroxysuccinimide (EDC/NHS, 1:2) were prepared in PBS at 0.1 mg·μL^{-1}. Bovine serum albumin (BSA) was prepared at 0.1% (*w*/*v*) in PBS and 1% (*v*/*v*) Tween 20%. H_2SO_4 was prepared into a 0.5 mol·L^{-1} solution, which was used to pretreat the sensing substrate before the modifications. Moreover, potassium hexacyanoferrate (III) K_3[Fe (CN)$_6$] and potassium hexacyanoferrate (II) K_4[Fe (CN)$_6$] were used to prepare a 1 mmol·L^{-1} [Fe (CN)$_6$]$^{3-/4-}$ solution in 5 mmol·L^{-1} PBS containing 0.1 mol·L^{-1} KCl. The NanoMIP as well as non-imprinted polymer nanoparticles (NIPnps, built of the same material as the NanoMIP) were acquired from MIP Discovery (Bedfordshire, UK), and diluted at 1:10 (*v*/*v*) in PBS. All solutions, except the NanoMIP, [Fe (CN)$_6$]$^{3-/4-}$ and H_2SO_4, were freshly prepared before analysis. All reagents were purchased from Sigma and were of analytical grade when applicable. Furthermore, all aqueous solutions were prepared with ultrapure water.

2.2. Antigens and Recombinant Antibodies

In this work, SARS-CoV-2 spike glycoprotein RBD was used as antigen, and was purchased from Native Antigen Company (Oxford, UK). The recombinant monoclonal antibodies herein used were of immunoglobulin G-class, namely: R107, RBD1106, and RBD5305, and were kindly provided by MIP Discovery (Bedfordshire, UK).

2.3. Gold Electrodes Pretreatment in Acid Solution

The BioS used in this work was based on gold screen-printed electrodes (Au-SPE). The Au-SPE comprised three electrodes, namely: working (Au), counter (Au), and reference (AgCl ink). Au-SPE were purchased from Metrohm, DropSens (model DRP-250AT). All Au-SPE were subjected to pretreatment on H_2SO_4 solution at 0.5 mol·L^{-1}. For this purpose, 50 μL of the solution was carefully dropped atop the Au-SPE, covering all electrodes. Thereafter, two voltametric assays were conducted in a row. The first pretreatment assay consisted of single-scan fast-cyclic voltammetry (CV), whose conditions were: preconditioning at an electric potential (*E*) of +2.0 V for 5 s; *E* deposition set to −0.35 V for 10 s; 3 s of equilibration between the *E* window of −0.30 V and +1.55 V; and *E* step of 0.001 V. The resulting rate was set to 4.0 V·s^{-1}. Following the first pretreatment step, the second protocol employed a standard CV, which was performed for 4 cycles. The settings for the standard CV were: 2 s of equilibration between the *E* window of −0.30 V and +1.55 V. The *E* step was set to 0.001 V and the scan rate was set to 0.1 V·s^{-1}.

2.4. Gold Substrate Modification

The surface modification herein selected was based on the spontaneous formation of self-assembled monolayers (SAM) on gold [29], and was followed by a crosslinking protocol based on EDC/NHS chemistry [30,31]. The SAM-forming domain herein selected was MUDA, whose aliphatic long chains have been reported to allow adequate anchoring of macromolecules such as antibodies onto surfaces [32]. Owing to the terminal carboxylic motif in MUDA, this compound is therefore compatible with EDC/NHS, which drove us to select this crosslinking method in our study. Furthermore, EDC/NHS is also compatible with the primary amines of amino acid residues in the antibodies, as well as the primary amines of the NanoMIP and NIPnps (information disclosed by the manufacturer).

The pretreated Au-SPE was modified by sequential drop-casting protocols. Between each step, the electrodes were thoroughly rinsed with ultrapure water and dried with a

nitrogen jet. The volume for the drop-casting was 50 µL, which was enough to cover all electrodes. The SPE was stored inside glass Petri dishes, which were laid horizontally on a flat surface. The incubations were performed either at 4 °C in the fridge (MUDA and BSA steps), or at room temperature (EDC/NHS and Antibody/NanoMIP step) The first step consisted of adding the MUDA solution, followed by 1 h incubation. The second step consisted of adding the EDC/NHS followed by 1 h incubation. The third step consisted of adding either the antibody or NanoMIP, or NIPnps solution, followed by 2 h incubation. The fourth and final step consisted of adding PBS, followed by 1 h incubation. BSA was herein used as a blocking agent, in order to block unbound sites and minimize responses due to the unspecific binding of targets on the gold substrate. The NIPnps were herein used as a control, as it is expected to yield no response, hence it is not imprinted with the target ultrastructural features. An overview of the surface modification protocol herein used, taking the modification with NanoMIP as an example, is showcased in Figure 1.

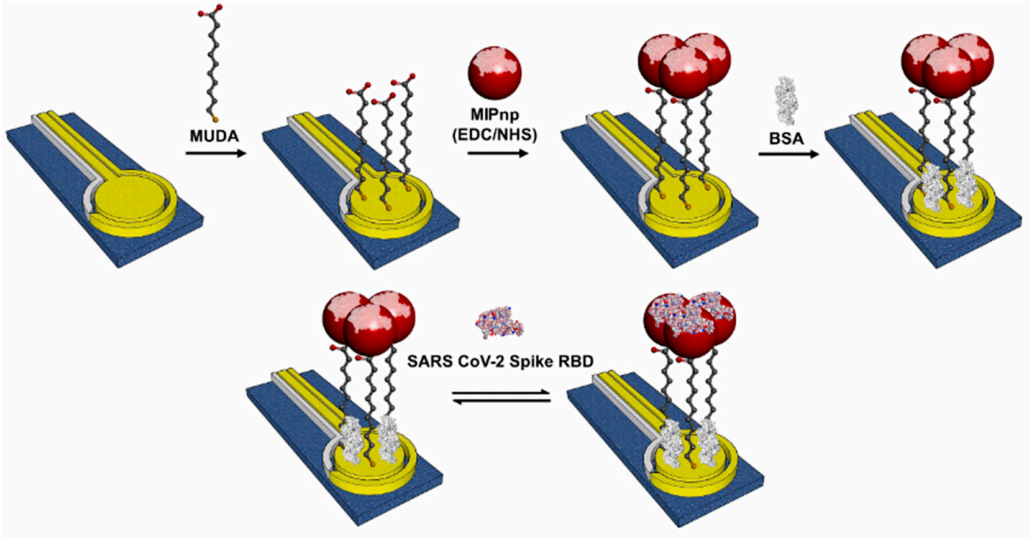

Figure 1. Surface modification protocol of the Au-SPE with MUDA, NanoMIP (crosslinked atop MUDA through EDC/NHS chemistry), and BSA. The rebinding of SARS-CoV-2 spike glycoprotein is therein indicated through reversible arrows, within the imprinted cavities towards the RBD of the SARS-CoV-2 spike glycoprotein.

Each step of surface modification was monitored up to the final sensor, and all-electric parameters were derived from the EIS assays and used to compare the behavior of each surface prior to exposure to the SARS-CoV-2 spike glycoprotein.

2.5. Impedimetric BioS Exposure to SARS-CoV-2 Spike Glycoprotein

Following the characterization of the surfaces, each sensor was individually exposed to undiluted SARS-CoV-2 spike antigen through a drop-casting protocol, and incubated at room temperature for 15 min. The total volume of the drop-casting was 10 µL, and only the working electrode was covered. Following the exposure, the electrodes were thoroughly rinsed with ultrapure water and dried with a nitrogen jet. All assays were performed in triplicates, using freshly prepared BioS.

2.6. Electrochemical Assays

Owing to the superficial nature of the binding of the antigens to the modified surfaces, we herein decided to employ EIS as the analytical method. Moreover, EIS was also used to monitor the modification process. The experimental conditions for EIS were: 5 s of equilibration time; frequency range of 0.1 to 10 kHz; direct current potential of +0.14 V and alternating current potential of 5 mV. The assays were performed in ferrocyanide solution (50 µL covering all electrodes).

The EIS Nyquist plot was used to gather electric information on the sensing surfaces, moreover, equivalent circuits were proposed according to the Randles equivalent topology [33,34]. This classic circuit comprises the resistance of the solution (R_s) in series with the capacitance of the double layer (C_{dl}), the latter of which is in parallel with the resultant of the series association of charge transfer resistance (R_{ct}) and Warburg diffusion element (W). A slight variation of this circuit was also used to model the electric behavior of the BioS, wherein the C_{dl} was swapped for a constant-phase element (CPE). This was performed due to the fact that CPE is reported to better describe the conductive and dielectric properties of solid electrodes [35]. The circuits herein used in the fitting are shown in Figure 2.

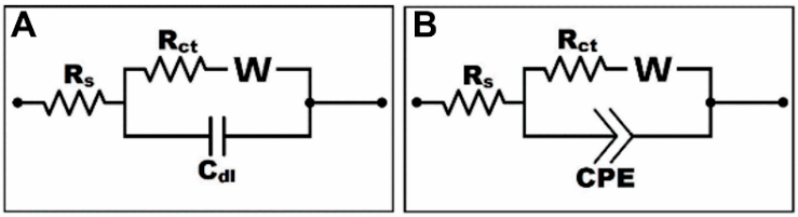

Figure 2. Randles equivalent circuit considering: (**A**) C_{dl} and (**B**) CPE.

3. Results

3.1. Electrochemical Features of the Modified Surfaces

In order to monitor the surface modification, as well as to characterize the electrochemical behavior of the BioS, EIS was used. The Nyquist plots of the experiments are shown in Figure 3, while the extracted circuit elements are disclosed in Table 1.

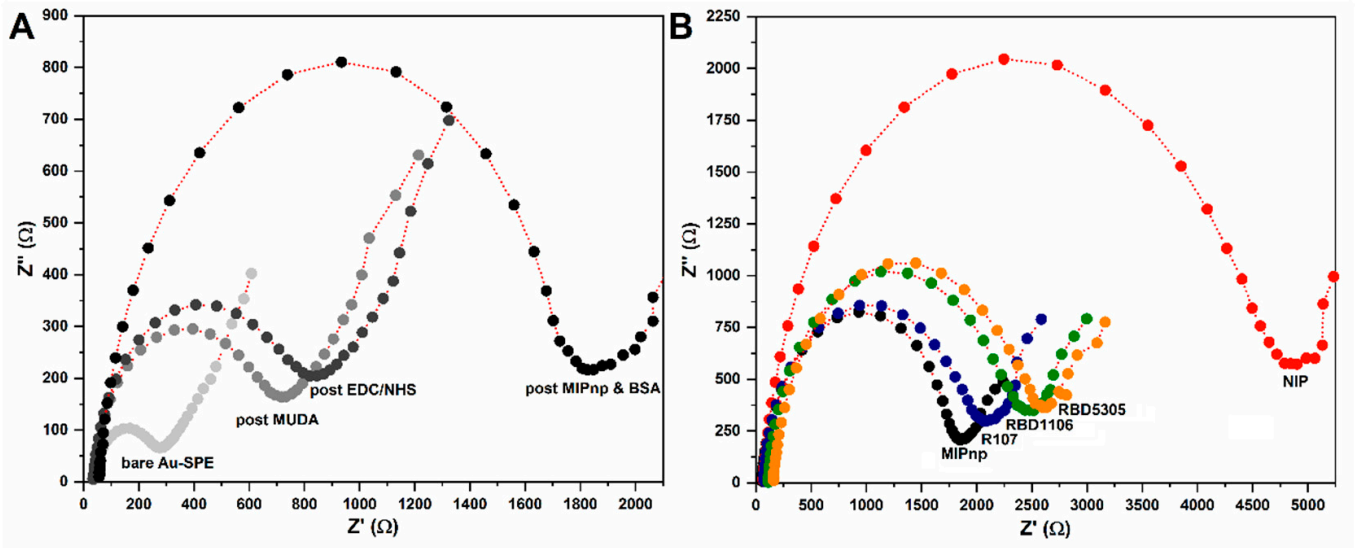

Figure 3. Nyquist plots of the electrochemical responses of the electrodes after each modification. the final modification therein represented regards the NanoMIP post-BSA-blocking, which was added to provide a sense of scaling (**A**). Nyquist plots of the BioS after preparation and BSA-blocking (**B**).

Table 1. Values of the equivalent circuit fitting of each surface modification step required for crafting the BioS with the recombinant antibodies, NanoMIP and NIPnps. The phase-shift angle (Φ) was extracted from each fitting concerning CPE modeling of the conducting/dielectric behavior of the electrode surface. Moreover, the X^2 parameter was used to evaluate the quality of each fitting. All resistances are in Ω and capacitances in nF.

Surface Modification Steps					
	R_{ct} (Ω)	**C_{dl} (nF)**	**Φ**	**X^2 (C_{dl} fit)**	**X^2 (CPE fit)**
AuSPE	222.3	5333	0.906	0.0027	0.0007
MUDA	616.4	5231	0.936	0.0031	0.0007
EDC/NHS	724.6	5209	0.931	0.0040	0.0009
Immunosensor Response Post BSA-Blocking					
	R_{ct} (Ω)	**C_{dl} (nF)**	**Φ**	**X^2 (C_{dl} fit)**	**X^2 (CPE fit)**
MIP	1687	2292	0.950	0.0028	0.0005
NIP	4458	1865	0.933	0.0087	0.0002
R107	1809	2362	0.970	0.0017	0.0007
RBD 1106	2161	2579	0.948	0.0022	0.0003
RBD 5305	2286	2507	0.930	0.0032	0.0004

Results evidenced that the semicircle of the Nyquist plots increased in diameter upon each step, which is suggestive of successful modification [4]. Moreover, the electrochemical behavior of the BioS differed from each other, being the smallest semicircle that of the NanoMIP, followed by the antibody-based BioS R107, RBD1106, and RBD5305. The longest semicircle diameter was that of the NIPnps. Parallelly, the fitted circuit components evidenced the increase in R_{ct} according to each successive modification step. Furthermore, all responses were in consonance with the behavior of solid electrodes, hence the resistive behavior denounced by the Φ values next to 1.0 [35]; and all fittings showcased adequate quality (Figure 3 and Table 1).

The increase in semicircle diameter is extensively reported as strong evidence of successful modification, due to its relationship with R_{ct} [36]. Considering that all surface modifiers herein used are of dielectric nature, an increase in the R_{ct} is expected, as the charge transfer is hindered on the surface of the electrode. In fact, the semicircle diameter of bare Au-SPE increased about 400 Ω upon the addition of MUDA, whose long aliphatic chains are known to promote a drop in conductivity upon its anchoring to surfaces [32]. On the other hand, the short-chained NHS promoted an increase of about 100 Ω upon its binding to the MUDA-modified Au-SPE, thence suggesting that smaller dielectric materials promote lesser hindrance to charge-transfer; which is extensively supported by the literature [37,38].

Following the modification with the recombinant antibodies, NanoMIP and NIPnps, an increase of the semicircle diameter, and consequently, of R_{ct} was noticed. The smaller increase of the semicircle regarding NanoMIP in comparison to the other molecules could be attributed to the size of the nanoparticles (40–80 nm range) and their homogeneous anchoring to the surface [39], nevertheless, further testing would be required to confirm this. Following the same interpretation, the longer semicircle diameter of the NIPnps suggests that the absence of imprinted cavities somehow hinders the access of the redox probe to the surface of the working electrode, thereby leading to an increase in the semicircle profile, and an apparent increase in the R_{ct}.

Conversely to the observed trends regarding R_{ct}, the C_{dl} values seemed to be consistent in the order of 5200–5300 nF in the first modification steps, though decreased by half upon the addition of the macromolecules. This is a remarkable finding, as it suggests that the capacitance values may be somehow correlated to the ultrastructural ordering of the electrode surface. In fact, this interpretation is supported by literature, as several authors have reported that the bulkiness of macromolecules disrupts the homogeneous formation of the Helmholtz Layer, which could strengthen the imperfect capacitive behavior, and change the predicted capacitance values [40,41].

In pursuance of exploring further the effect of surface modifications on the electric parameters of the electrodes, the R_{ct} values were plotted against the C_{dl}, so to highlight if there could be any trend between them. Results are depicted in Figure 4.

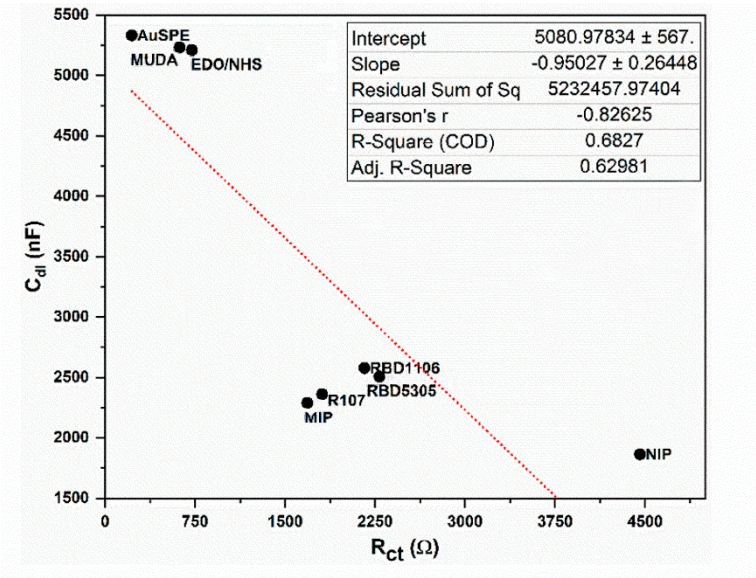

Figure 4. Plot of C_{dl} versus R_{ct}. The inset details the linear fitting herein used, being the r2 of −0.8262. Data which showcased overlap: upper-left corner: MUDA and EDC/NHS; lower-central region: RBD 1106 and RBD 5305, as well as R 107 and MIP.

Results evidenced that there seems to be an inversely proportional trend between the C_{dl} and R_{ct} values. Moreover, the plotting of these two attributes allowed visual segregation of the dataset from the modification steps (upper-left corner), and the dataset of the BioS based on NanoMIP and recombinant antibodies (lower-central part), and NIPnps (lower-right corner).

The seemingly inversely proportional trends of the C_{dl} and R_{ct} values are known to occur in many systems in electrochemistry [42]. The R_{ct} values are regarded as descriptors of not only hindrances to charge transfer on electrode surfaces, but also may provide information on the accessibility of the solvent, as they carry the redox probes used in most reported EIS assays [43,44]. Likewise, owing to the formation of the double layer in the surface solid electrodes upon contact with a liquid medium, the capacitance values also provide information on the interface and its integrity [45]. Although the implications of the relationship between R_{ct} and C_{dl} are not fully known, our results hinted that they could harness information to allow the discrimination of the origin of the dataset, thereby possibly serving as a characterization tool.

3.2. Comparison of Immunosensor Response

After evaluating the electrochemical behavior of the BioS during their manufacturing, their responses were tested upon the presence of SARS-CoV-2 spike glycoprotein. The analytical signal herein taken was the variation of R_{ct}, hence many other authors have disclosed this parameter as a reliable analytical descriptor in EIS. Results are depicted in Figure 5.

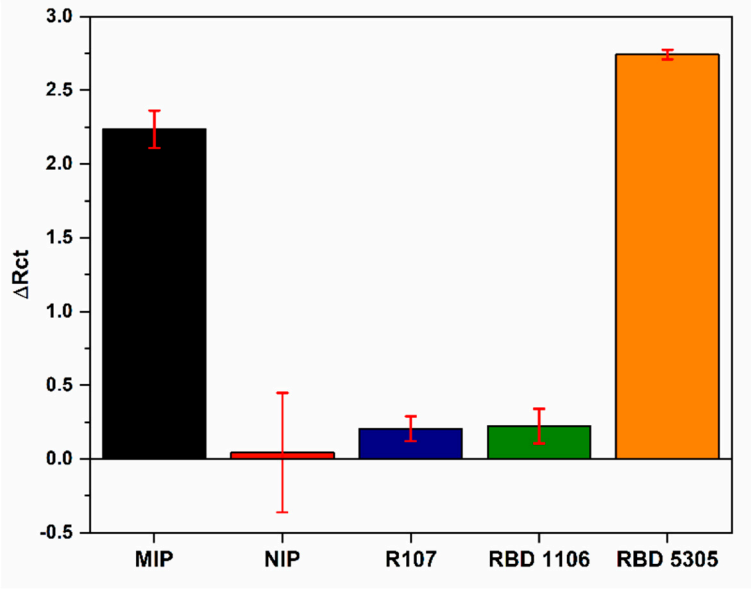

Figure 5. Response of the BioS after incubation with SARS-CoV-2 spike glycoprotein. The analytical signal is herein represented as a relative increase in charge-transfer resistance (ΔR_{ct}).

Results showed that the recombinant monoclonal antibody RBD 5305 yields the highest change in signal upon incubation with SARS-CoV-2 spike glycoprotein. The NanoMIP exhibited the second highest change in signal, followed by the RBD1106 and R107. The response of the NIP was unreliable, as hinted by the long error bars, and was seemingly the lowest (Figure 5).

The remarkable affinity of RBD-based antibodies towards SARS-CoV-2 spike glycoprotein has been previously reported and is considered crucial in the development of BioS and therapeutic strategies [46]. RBD5305 is a full-sized chimeric recombinant monoclonal antibody, which is expressed in mammalian cells. This monoclonal antibody is based upon the combination of original wild-type variable domains of rat monoclonal antibodies and human immunoglobulin 1 constant domains [47]. On the other hand, RBD1106 and R107 are hybridoma clones from Sp2/0 myeloma and spleen cells of BALB/C mice that were immunized with recombinant SARS-CoV-2 Spike RBD [47]. These recombinant antibodies have been proven in vitro as efficient inhibitors of the interaction between recombinant RBD and the angiotensin-converting enzyme 2 [48,49], which is a critical step in the infection of cells.

The order of affinity between the monoclonal antibodies and the β variant of SARS-CoV-2 spike glycoprotein is RBD1106 > RBD5305 > RBD107. These findings differed from what was obtained by the electrochemical BioS; hence the best response came from the modification that was conducted with RBD5305. The main feature of the β variant is that it has four mutations in its spike protein, namely: K417N, E484K, N501Y, and D614G [47]. Nevertheless, factors other than affinity could play a role in the electrochemical response, such as successful anchoring to the surface. To all accounts, RBD5305 showed the best results in the conditions herein tested.

In a similar way to RBD5305, the NanoMIP showcased a striking increase in the signal upon being exposed to the target. This result may be hence the imprinted cavities in the NanoMIP bear the same ultrastructural topology of SARS-CoV-2 spike glycoprotein RBD. To all accounts, the reported affinity constants of the NanoMIP used in this work were $\leq$18 nM to SARS-CoV-2 spike glycoprotein, and heat-transfer-based immunosensors exhibited very low limits of detection to both the α ($\sim$9.9 fg·mL^{-1}) and Δ ($\sim$6.1 fg·mL^{-1}) variants of the spike glycoprotein [50]. Nonetheless, the different responses of the NanoMIP and NIPnps hint at the effect that the imprinted cavities have on the performance of the sensor, hence the varied response in the assays with the NIPnps strongly hinted at an unspecific binding. Overall, it has to be remarked that the NanoMIP response is comparable to that of a widely

used, and reliable, recombinant monoclonal antibody in the development of impedimetric immunosensors for SARS-CoV-2 spike glycoprotein, thus demonstrating the nature of plastic antibodies of synthetic receptors prepared by molecular imprinting technology.

4. Conclusions

This work compared the electrochemical behavior of impedimetric BioS based on recombinant antibodies and nanoMIPs to detect SARS-CoV-2 spike glycoprotein. Results showed that the surface modification protocol based on MUDA and crosslinking with EDC/NHS was successful, as the semicircle diameter of the Nyquist plots of EIS increased upon each modification, which suggests the increase of R_{ct} due to the binding of dielectric materials on the conductive surface. Moreover, the R_{ct} and C_{dl} values followed a seemingly inversely-proportional trend, and their datasets allowed the differentiation of the origin of the observations, thereby suggesting that this strategy could be used for characterization purposes. Furthermore, the type of receptors used to craft the sensor led to very distinct responses, the RBD5305, and the NanoMIP-based BioS showcased the highest increment of signal in the conditions herein reported, which suggests their adequacy in the development of impedimetric immunosensors for SARS-CoV-2 spike glycoprotein.

Author Contributions: Conceptualization: D.V.T., R.G., G.M.T., C.M. and E.M. Methodology: D.V.T. and R.G. Investigation, D.V.T. and R.G. Resources: G.M.T. and E.M. Writing, editing and review: D.V.T., R.G., G.M.T. and E.M. Supervision: G.M.T., C.M. and E.M. All authors have read and agreed to the published version of the manuscript.

Funding: This research was funded by the Department of Biomedical, Surgical and Dental Sciences of Università di Milano (Piano di Sostegno alla Ricerca, PSR2020_DIP_017). D.V.T. was a postdoctoral researcher at the Department of Biological and Environmental Sciences & Technologies (Di. S. Te. B. A.) of the University of Salento and held a grant in the scientific sector CHIM/01 funded by the call Dipartimenti di Eccellenza 2018–2022—CUP: F85D1800013000.

Institutional Review Board Statement: Not applicable.

Informed Consent Statement: Not applicable.

Data Availability Statement: Not applicable.

Acknowledgments: During D.V.T. research activities at the Department of Biological and Environmental Sciences & Technologies (Di. S. Te. B. A.) of the University of Salento, he held a grant in the scientific sector CHIM/01 funded by the call Dipartimenti di Eccellenza 2018–2022—CUP: F85D1800013000. Furthermore, the authors would like to thank MIP Discovery.

Conflicts of Interest: The authors declare no conflict of interest.

References

1. Choi, J.R. Development of Point-of-Care Biosensors for COVID-19. *Front. Chem.* **2020**, *8*, 517. [CrossRef] [PubMed]
2. Antunes, R.S.; Thomaz, D.V.; Garcia, L.F.; Gil, E.D.S.; Lopes, F.M. Development and Optimization of Solanum Lycocarpum Polyphenol Oxidase-Based Biosensor and Application towards Paracetamol Detection. *Adv. Pharm. Bull.* **2020**, *11*, 469–476. [CrossRef]
3. Thomaz, D.V. Development of Laccase-TiO2@Carbon Paste Biosensor for Voltammetric Determination of Paracetamol. *Int. J. Electrochem. Sci.* **2018**, *13*, 10884–10893. [CrossRef]
4. Antunes, R.S.; Thomaz, D.V.; Garcia, L.F.; Gil, E.D.S.; Sommerset, V.S.; Lopes, F.M. Determination of Methyldopa and Paracetamol in Pharmaceutical Samples by a Low Cost Genipa americana L. Polyphenol Oxidase Based Biosensor. *Adv. Pharm. Bull.* **2019**, *9*, 416–422. [CrossRef] [PubMed]
5. Khodami, M.; Hirbodvash, Z.; Krupin, O.; Wong, W.R.; Lisicka-Skrzek, E.; Northfield, H.; Hahn, C.; Berini, P. Fabrication of Bloch Long Range Surface Plasmon Waveguides Integrating Counter Electrodes and Microfluidic Channels for Multimodal Biosensing. *J. Microelectromech. Syst.* **2021**, *30*, 686–695. [CrossRef]
6. Kim, J.H.; Suh, Y.J.; Park, D.; Yim, H.; Kim, H.; Kim, H.J.; Yoon, D.S.; Hwang, K.H. Technological advances in electrochemical biosensors for the detection of disease biomarkers. *Biomed. Eng. Lett.* **2021**, *11*, 309–334. [CrossRef] [PubMed]
7. Hedayatipour, A.; Mcfarlane, N. Wearables for the Next Pandemic. *IEEE Access* **2020**, *8*, 184457–184474. [CrossRef]
8. Malon, R.S.P.; Sadir, S.; Balakrishnan, M.; Córcoles, E.P. Saliva-Based Biosensors: Noninvasive Monitoring Tool for Clinical Diagnostics. *BioMed Res. Int.* **2014**, *2014*, 962903. [CrossRef]

9. Malamud, D. Saliva as a Diagnostic Fluid. *Dent. Clin. N. Am.* **2011**, *55*, 159–178. [CrossRef]
10. Goldoni, R.; Scolaro, A.; Boccalari, E.; Dolci, C.; Scarano, A.; Inchingolo, F.; Ravazzani, P.; Muti, P.; Tartaglia, G. Malignancies and biosensors: A focus on oral cancer detection through salivary biomarkers. *Biosensors* **2021**, *11*, 396. [CrossRef]
11. Goldoni, R.; Dolci, C.; Boccalari, E.; Inchingolo, F.; Paghi, A.; Strambini, L.; Galimberti, D.; Tartaglia, G.M. Salivary biomarkers of neurodegenerative and demyelinating diseases and biosensors for their detection. *Ageing Res. Rev.* **2022**, *76*, 101587. [CrossRef] [PubMed]
12. Goldoni, R.; Farronato, M.; Connelly, S.T.; Tartaglia, G.M.; Yeo, W.H. Recent advances in graphene-based nanobi-osensors for salivary biomarker detection. *Biosens. Bioelectron.* **2021**, *171*, 112723. [CrossRef]
13. Nascimento, E.D.; Fonseca, W.T.; de Oliveira, T.R.; de Correia, C.R.; Faça, V.M.; de Morais, B.P.; Silvestrini, V.C.; Pott-Junior, H.; Teixeira, F.R.; Faria, R.C. COVID-19 diagnosis by SARS-CoV-2 Spike protein detection in saliva using an ultrasensitive magneto-assay based on disposable electrochemical sensor. *Sens. Actuators B Chem.* **2021**, *353*, 131128. [CrossRef] [PubMed]
14. Rasmi, Y.; Li, X.; Khan, J.; Ozer, T.; Choi, J.R. Emerging point-of-care biosensors for rapid diagnosis of COVID-19: Current progress, challenges, and future prospects. *Anal. Bioanal. Chem.* **2021**, *413*, 4137–4159. [CrossRef] [PubMed]
15. Zhang, M.; Li, X.; Pan, J.; Zhang, Y.; Zhang, L.; Wang, C.; Yan, X.; Liu, X.; Lu, G. Ultrasensitive detection of SARS-CoV-2 spike protein in untreated saliva using SERS-based biosensor. *Biosens. Bioelectron.* **2021**, *190*, 113421. [CrossRef]
16. Cerutti, F.; Burdino, E.; Milia, M.G.; Allice, T.; Gregori, G.; Bruzzone, B.; Ghisetti, V. Urgent need of rapid tests for SARS CoV-2 antigen detection: Evaluation of the SD-Biosensor antigen test for SARS-CoV-2. *J. Clin. Virol.* **2020**, *132*, 104654. [CrossRef]
17. Kopel, J.; Goyal, H.; Perisetti, A. Antibody tests for COVID-19. *Bayl. Univ. Med. Cent. Proc.* **2020**, *34*, 63–72. [CrossRef]
18. Ning, L.; Abagna, H.B.; Jiang, Q.; Liu, S.; Huang, J. Development and application of therapeutic antibodies against COVID-19. *Int. J. Biol. Sci.* **2021**, *17*, 1486–1496. [CrossRef]
19. Ma, H.; Ó'Fágáin, C.; O'Kennedy, R. Antibody stability: A key to performance—Analysis, influences and improvement. *Biochimie* **2020**, *177*, 213–225. [CrossRef]
20. Luan, J.; Xu, T.; Cashin, J.; Morrissey, J.J.; Kharasch, E.D.; Singamaneni, S. Environmental Stability of Plasmonic Biosensors Based on Natural versus Artificial Antibody. *Anal. Chem.* **2018**, *90*, 7880–7887. [CrossRef]
21. Uzun, L.; Turner, A.P. Molecularly-imprinted polymer sensors: Realising their potential. *Biosens. Bioelectron.* **2016**, *76*, 131–144. [CrossRef] [PubMed]
22. Zidarič, T.; Finšgar, M.; Maver, U.; Maver, T. Artificial Biomimetic Electrochemical Assemblies. *Biosensors* **2022**, *12*, 44. [CrossRef] [PubMed]
23. Ziqi, W.; Kai, C.; Costabel, U.; Xiaoju, Z. Nanotechnology-facilitated vaccine development during the coronavirus disease 2019 (COVID-19) pandemic. *Exploration* **2022**, *2022*, 20210082. [CrossRef] [PubMed]
24. Malitesta, C.; Mazzotta, E.; Picca, R.A.; Poma, A.; Chianella, I.; Piletsky, S.A. MIP sensors—The electrochemical approach. *Anal. Bioanal. Chem.* **2012**, *402*, 1827–1846. [CrossRef]
25. Goldoni, R.; Thomaz, D.V.; Di Giulio, T.; Malitesta, C.; Mazzotta, E. An insight into polyscopoletin electrosynthesis by a quality-by-design approach. *J. Mater. Sci.* **2022**, *57*, 12161–12175. [CrossRef] [PubMed]
26. El-Schich, Z.; Zhang, Y.; Feith, M.; Beyer, S.; Sternbæk, L.; Ohlsson, L.; Stollenwerk, M.; Wingren, A.G. Molecularly imprinted polymers in biological applications. *BioTechniques* **2020**, *69*, 406–419. [CrossRef]
27. Raziq, A.; Kidakova, A.; Boroznjak, R.; Reut, J.; Öpik, A.; Syritski, V. Development of a portable MIP-based electrochemical sensor for detection of SARS-CoV-2 antigen. *Biosens. Bioelectron.* **2021**, *178*, 113029. [CrossRef]
28. Ratautaite, V.; Boguzaite, R.; Brazys, E.; Ramanaviciene, A.; Ciplys, E.; Juozapaitis, M.; Slibinskas, R.; Bechelany, M.; Ramanavicius, A. Molecularly imprinted polypyrrole based sensor for the detection of SARS-CoV-2 spike glycoprotein. *Electrochim. Acta* **2022**, *403*, 139581. [CrossRef]
29. Brothers, M.C.; Moore, D.; Lawrence, M.S.; Harris, J.; Joseph, R.M.; Ratcliff, E.; Ruiz, O.N.; Glavin, N.; Kim, S.S. Impact of Self-Assembled Monolayer Design and Electrochemical Factors on Impedance-Based Biosensing. *Sensors* **2020**, *20*, 2246. [CrossRef]
30. Yüce, M.; Kurt, H. How to make nanobiosensors: Surface modification and characterisation of nanomaterials for biosensing applications. *RSC Adv.* **2017**, *7*, 49386. [CrossRef]
31. Adamiak, K.; Sionkowska, A. Current methods of collagen cross-linking: Review. *Int. J. Biol. Macromol.* **2020**, *161*, 550–560. [CrossRef] [PubMed]
32. Berchmans, S.; Nirmal, R.G.; Prabaharan, G.; Mishra, A.K.; Yegnaraman, V. Solution phase electron transfer versus bridge mediated electron transfer across carboxylic acid terminated thiols. *J. Solid State Electrochem.* **2005**, *10*, 439–446. [CrossRef]
33. Lai, C.-Y.; Huang, W.-C.; Weng, J.-H.; Chen, L.-C.; Chou, C.-F.; Wei, P.-K. Impedimetric aptasensing using a symmetric Randles circuit model. *Electrochim. Acta* **2020**, *337*, 135750. [CrossRef]
34. Antunes, R.S.; Ferraz, D.; Garcia, L.F.; Thomaz, D.V.; Luque, R.; Lobón, G.S.; Gil, E.D.S.; Lopes, F.M. Development of a Polyphenol Oxidase Biosensor from Jenipapo Fruit Extract (Genipa americana L.) and Determination of Phenolic Compounds in Textile Industrial Effluents. *Biosensors* **2018**, *8*, 47. [CrossRef]
35. Lasia, A. The Origin of the Constant Phase Element. *J. Phys. Chem. Lett.* **2022**, *13*, 580–589. [CrossRef] [PubMed]
36. Morales, M.A.; Paiva, W.A.; Marvin, L.; Balog, E.R.M.; Halpern, J.M. Electrochemical characterization of the stimuli-response of surface-immobilized elastin-like polymers. *Soft Matter* **2019**, *15*, 9640–9646. [CrossRef]

37. Guler, Z.; Sarac, A. Electrochemical impedance and spectroscopy study of the EDC/NHS activation of the carboxyl groups on poly(ε-caprolactone)/poly(m-anthranilic acid) nanofibers. *Express Polym. Lett.* **2016**, *10*, 96–110. [CrossRef]
38. Gogola, J.L.; Martins, G.; Caetano, F.R.; Ricciardi-Jorge, T.; dos Santos, C.N.D.; Marcolino-Junior, L.H.; Bergamini, M.F. Label-free electrochemical immunosensor for quick detection of anti-hantavirus antibody. *J. Electroanal. Chem.* **2019**, *842*, 140–145. [CrossRef]
39. Córdoba-Torres, P.; Mesquita, T.J.; Nogueira, R.P. Relationship between the Origin of Constant-Phase Element Behavior in Electrochemical Impedance Spectroscopy and Electrode Surface Structure. *J. Phys. Chem. C* **2015**, *119*, 4136–4147. [CrossRef]
40. Xu, Y.; Li, C.; Jiang, Y.; Guo, M.; Yang, Y.; Yang, Y.; Yu, H. Electrochemical Impedance Spectroscopic Detection of *E.coli* with Machine Learning. *J. Electrochem. Soc.* **2020**, *167*, 047508. [CrossRef]
41. Xu, X.; Makaraviciute, A.; Kumar, S.; Wen, C.; Sjödin, M.; Abdurakhmanov, E.; Danielson, U.H.; Nyholm, L.; Zhang, Z. Structural Changes of Mercaptohexanol Self-Assembled Monolayers on Gold and Their Influence on Impedimetric Aptamer Sensors. *Anal. Chem.* **2019**, *91*, 14697–14704. [CrossRef] [PubMed]
42. Dhillon, S.; Kant, R. Theory for electrochemical impedance spectroscopy of heterogeneous electrode with distributed capacitance and charge transfer resistance. *J. Chem. Sci.* **2017**, *129*, 1277–1292. [CrossRef]
43. Kondo, Y.; Fukutsuka, T.; Yokoyama, Y.; Miyahara, Y.; Miyazaki, K.; Abe, T. Kinetic properties of sodium-ion transfer at the interface between graphitic materials and organic electrolyte solutions. *J. Appl. Electrochem.* **2021**, *51*, 629–638. [CrossRef]
44. Hauch, A.; Georg, A. Diffusion in the electrolyte and charge-transfer reaction at the platinum electrode in dye-sensitized solar cells. *Electrochim. Acta* **2001**, *46*, 3457–3466. [CrossRef]
45. Cuentas-Gallegos, A.; Rayón-López, N.; Mejía, L.; Vidales, H.V.; Miranda-Hernández, M.; Robles, M.; Muńiz-Soria, J. Porosity and Surface Modifications on Carbon Materials for Capacitance Improvement. *Open Mater. Sci.* **2016**, *3*, 51. [CrossRef]
46. Tai, W.; He, L.; Zhang, X.; Pu, J.; Voronin, D.; Jiang, S.; Zhou, Y.; Du, L. Characterization of the receptor-binding domain (RBD) of 2019 novel coronavirus: Implication for development of RBD protein as a viral attachment inhibitor and vaccine. *Cell. Mol. Immunol.* **2020**, *17*, 613–620. [CrossRef]
47. HyTest. HyTest SARS-CoV-2 Antibodies and Detection of Variants. 2022. pp. 4–8. Available online: https://shop.hytest.fi/spree/products/4162/SARS-CoV-2_detection_of_variants.pdf?1648709970 (accessed on 24 August 2022).
48. Chen, J.; Wu, F.; Lin, D.; Kong, W.; Cai, X.; Yang, J.; Sun, X.; Cao, P. Rational optimization of a human neutralizing antibody of SARS-CoV-2. *Comput. Biol. Med.* **2021**, *135*, 104550. [CrossRef]
49. HyTest. Reagents for SARS-CoV-2 Antigen and Antibody Assays. 2020. Available online: https://shop.hytest.fi/spree/products/4161/SARS-CoV-2_TechNotes_%282%29.pdf?1648709956 (accessed on 24 August 2022).
50. McClements, J.; Bar, L.; Singla, P.; Canfarotta, F.; Thomson, A.; Czulak, J.; Johnson, R.E.; Crapnell, R.D.; Banks, C.E.; Payne, B.; et al. Molecularly Imprinted Polymer Nanoparticles Enable Rapid, Reliable, and Robust Point-of-Care Thermal Detection of SARS-CoV-2. *ACS Sens.* **2022**, *7*, 1122–1131. [CrossRef]